Check for updates

Received: 2 February 2022 | Revised: 20 March 2022 | Accepted: 31 March 2022

DOI: 10.1002/idm2.12026

RESEARCH ARTICLE

Interdisciplinary Materials — Open Access — WILEY

Bioinspired cellulose-integrated MXene-based hydrogels for multifunctional sensing and electromagnetic interference shielding

Jingjiang Wei[1,2] | **Chenglong Zhu**[1] | **Zhihui Zeng**[3] | **Fei Pan**[4] | **Fuqiang Wan**[1] | **Liwen Lei**[1] | **Gustav Nyström**[2,5] | **Zhengyi Fu**[1]

[1]State Key Laboratory of Advanced Technology for Materials Synthesis and Processing, Wuhan University of Technology, Wuhan, Hubei, PR China

[2]Laboratory for Cellulose and Wood Materials, Swiss Federal Laboratories for Materials Science and Technology (Empa), Dübendorf, Switzerland

[3]Key Laboratory for Liquid-Solid Structural Evolution and Processing of Materials, School of Material Science and Engineering, Shandong University, Jinan, Shandong, PR China

[4]Laboratory for Biointerfaces, Swiss Federal Laboratories for Materials Science and Technology (Empa), St. Gallen, Switzerland

[5]Department of Health Science and Technology, ETH Zürich, Zürich, Switzerland

Correspondence

Zhihui Zeng, Key Laboratory for Liquid-Solid Structural Evolution and Processing of Materials, School of Material Science and Engineering, Shandong University, Jinan 250061, Shandong, PR China.
Email: zhihui.zeng@sdu.edu.cn

Gustav Nyström, Laboratory for Cellulose and Wood Materials, Swiss Federal Laboratories for Materials Science and Technology (Empa), 8600 Dübendorf, Switzerland.
Email: gustav.nystroem@empa.ch

Zhengyi Fu, State Key Laboratory of Advanced Technology for Materials Synthesis and Processing, Wuhan University of Technology, Wuhan 430070, Hubei, PR China.
Email: zyfu@whut.edu.cn

Funding information

National Natural Science Foundation of China, Grant/Award Numbers: 51521001, 51832003, 51911530153

Abstract

Bioinspired hydrogels are complex materials with distinctive properties comparable to biological tissues. Their exceptional sensitivity to various external stimuli leads to substantial application potential in wearable smart devices. However, these multifaceted hydrogels are often challenging to be combined with pattern customization, stimulus responsiveness, self-healing, and biocompatibility. Herein, inspired by mussel secretions, a printable, self-healing, and biocompatible MXene-based composite hydrogel was designed and prepared by incorporating $Ti_3C_2T_x$ MXene nanosheets into the hydrogel framework through the chelation of calcium ions (Ca^{2+}) with polyacrylic acid and cellulose nanofibers at alkaline conditions. The biocompatible conductive hydrogel exhibited sensitivity (gauge factor of 2.16), self-healing (within 1 s), recognition, and adhesion, distinguishing it as an ideal candidate for wearable multifunctional sensors toward strain sensing, vocal sensing, signature detection, and Morse code transmission. Additionally, the multifunctional hydrogel manifested efficient electromagnetic interference shielding properties (reaching more than 30 dB at a thickness of 2.0 mm), protecting electronics and humans from electromagnetic radiation and pollution. Therefore, the presented work represents a versatile strategy for developing environmentally friendly conductive hydrogels, demonstrating the perspectives of intelligent hydrogels for multifunctional applications.

KEYWORDS

cellulose nanofiber, electromagnetic interference shielding, hydrogel, MXene, sensor

This is an open access article under the terms of the Creative Commons Attribution License, which permits use, distribution and reproduction in any medium, provided the original work is properly cited.

© 2022 The Authors. *Interdisciplinary Materials* published by Wuhan University of Technology and John Wiley & Sons Australia, Ltd.

2767441x, 2022, 4, Downloaded from https://onlinelibrary.wiley.com/doi/10.1002/idm2.12026 by Universitätsbibliothek Basel, Wiley Online Library on [02/11/2022]. See the Terms and Conditions (https://onlinelibrary.wiley.com/terms-and-conditions) on Wiley Online Library for rules of use; OA articles are governed by the applicable Creative Commons License

1 | INTRODUCTION

Over more than a billion years of natural evolution, living systems have developed various highly adaptable biological materials to respond to environmental changes, motivating scientists to design nature-inspired materials.[1–4] The research on the growth process and structure of biomaterials has led to a new research direction, "bioprocess-inspired fabrication," which guides the preparation of excellent multifunctional materials under mild environmental conditions.[5–7] One notable example in nature is mussels that can adhere tightly to foreign surfaces in seawater by secreting adhesive proteins.[8,9] This observation stimulated work on bioinspired hydrogels that manifest unparalleled and unique advantages. Bioinspired hydrogels have been widely investigated in drug release, antimicrobial wound dressings, tissue engineering, and adhesives owing to their high specific surface area, inherent wettability and softness, and excellent biocompatibility.[10–14] However, the preparation and processing procedure for these hydrogels are usually complicated, making them difficult to customize in complex patterns and thus hindering their practical applications.[15,16] Recently, the rapid development of additive manufacturing has made it an important state-of-the-art technology for functional material preparation. In particular, additive manufacturing technology based on extrusion three-dimensional (3D) printing has proved to be a very effective preparation technology for hydrogel materials, which has been widely applied in the fields of wearable smart devices, soft robots, and artificial organs.[17–19]

Hydrogel materials used for 3D printing usually need to meet some specific rheological properties, that is, an obvious shear-thinning behavior, storage (G') and loss (G'') modulus superior to 1000 Pa, and the G' greater than G'' in the low shear rate region, in addition to dynamic yield stress (τ_y) greater than 100 Pa.[20] Cellulose nanofibers (CNFs) are composed of a well-ordered, highly crystalline, arrangement of cellulose, the most abundant renewable natural polymers on earth. CNFs are widely known as rheology modifiers, which allow obtaining shear-thinning gels from Newtonian liquids because of their high strength, large aspect ratio, and abundant surface functional groups.[21,22] However, multiple technologies symbolizing current scientific advances, such as biointegrated electronics, water desalination, and biodegradable plastics, require materials combining several essential properties.[23–29] Moreover, bioinspired and adaptable hydrogels are highly desired to respond to external stimuli, such as pressure, temperature, light, electromagnetic fields, and pH.[30–34] Therefore, the introduction of functional nanomaterials is very important for the preparation of multifunctional intelligent hydrogels. Recently, the emerging $Ti_3C_2T_x$ MXenes, 2D transition metal carbide, nitride, and carbonitride confer outstanding electromagnetic interference (EMI) shielding properties.[35] Additionally, their large specific surface area and abundant surface functional groups (−OH, −F, −O, etc.) combined with their high electrical conductivity distinguish them as excellent candidates to enhance the mechanical and electrical properties of multifunctional hydrogels.[36,37]

Herein, a multifunctional and highly adaptable Ca-PAA-CNF-MXene hydrogel inspired by mussel secretions was developed through a facile preparation process. This hydrogel was designed by incorporating MXene nanosheets into a 3D network of chelates formed by polyacrylic acid (PAA) and CNF with calcium ions (Ca^{2+}) under alkaline conditions. The whole preparation was performed in ambient conditions without the need for specialized processing. Owing to the abundant carboxyl groups on the PAA chains,[38] carboxyl and hydroxyl groups on the CNF chains,[39] and various functional groups on the MXene surface,[36] the Ca-PAA-CNF-MXene composite hydrogel was formed by physical and chemical cross-linking, possessing many hydrogen, ionic, and covalent bonds, thus exhibiting excellent stretchability, plasticity, adhesion, 3D printability, self-healing, biocompatibility, and electrical conductivity. Moreover, when the printed hydrogel was encapsulated in a stretchable dielectric tape, a multifunctional sensor could be obtained to sensitively respond to external stimuli, displaying a relative resistance change. This multifunctional sensor could be implemented concurrently as a strain sensor, a voice sensor, a signature sensor, and a Morse code transmitter. Moreover, the moderate integration of water molecules, polymer matrices, and MXene within the porous structure in this hydrogel yields EMI shielding functionality. Consequently, this multifunctional hydrogel is promising for facilitating the development and application of bioinspired materials in the field of flexible, intelligent devices.

2 | EXPERIMENTAL SECTION

2.1 | Materials

PAA solution (average M_w ~250 000, 35 wt% in H_2O), lithium fluoride (LiF), and hydrochloric acid (HCl, 37%) were purchased from Sigma-Aldrich Trading Co., Ltd. Calcium chloride anhydrous ($CaCl_2$), sodium dodecylbenzene sulfonate (SDBS), and sodium hydroxide (NaOH) were supplied by Sinopharm Chemical Reagent

2767441x, 2022, 4, Downloaded from https://onlinelibrary.wiley.com/doi/10.1002/idm2.12026 by Universitätsbibliothek Basel, Wiley Online Library on [02/11/2022]. See the Terms and Conditions (https://onlinelibrary.wiley.com/terms-and-conditions) on Wiley Online Library for rules of use; OA articles are governed by the applicable Creative Commons License

Co., Ltd. Ti_3AlC_2 MAX was provided by Laizhou Kai Kai Ceramic Materials Co., Ltd., China. Carboxylated CNFs were purchased from Guilin Qihong Technology Co., Ltd. VHB tape was provided by 3 M China Co., Ltd. The used ultrapure water was prepared by the Millipore system (18.2 MΩ cm).

Fabrication of MXene nanomaterials. Briefly put, LiF (1 g) was added to a 20 ml HCl solution (9 M) and gently stirred until the LiF dissolved entirely, forming a clear mixed solution. Then, while vigorously stirring, Ti_3AlC_2 MAX (1 g) was slowly and carefully added to the mixture. After 24 h of etching at room temperature, the mixture was centrifuged for 5 min at 4000 rpm. After pouring the supernatant, the precipitate was redispersed with 40 ml deionized water. This centrifugation–redispersion procedure was repeated at least five times more until the suspension reached a pH value greater than 6. Subsequently, the precipitate was redispersed and vigorously shaken for 30 min. Finally, the dispersion was centrifuged at 5000 rpm for 30 min, and the final suspension was collected to get the delaminated $Ti_3C_2T_x$ MXene.

Preparation of Ca-PAA-CNF-MXene hydrogels. Ca-PAA-CNF-MXene hydrogels were produced by optimizing previously described techniques.[40–43] A total of 50 ml mixture A of NaOH (0.1 M) and CNF (0.02 g) was gradually added to another 50 ml mixture B of $CaCl_2$ (0.2 M) and PAA (0.2 M) containing MXene in various concentrations and SDBS (0.05 g). As mixture A was added dropwise, a black sticky hydrogel gradually formed in the beaker. Stirring continued for an extra 1 h to separate the black hydrogel from the clarifying solution. The suspension was then poured out and the black hydrogel was rinsed with deionized water, followed by a repetition of the cleaning procedure until the suspension became clear. Finally, the black product Ca-PAA-CNF-MXene hydrogel was obtained.

Fabrication of Ca-PAA-CNF-MXene strain sensor. First, two copper wires were attached to a stretchable dielectric layer (Very high bond [VHB] 4905) at specific positions. Then, an extrusion-based bio-3D printer was used to print Ca-PAA-CNF-MXene hydrogel into a grid pattern on VHB with copper wires. It is worth noting here that the hydrogel to be printed needs to be covered on copper wires. Finally, another layer of VHB of the same size was encapsulated to form a sandwich structure device.

2.2 | Mechanical tests

The rheological behavior of Ca-PAA, Ca-PAA-MXene, Ca-PAA-CNF, and Ca-PAA-CNF-MXene was investigated by a Thermo HAAKE MARS 60 machine using a 20 mm parallel plate. Dynamic frequency sweep was measured from 0.1 to 10 Hz at 25°C in the oscillation mode with a fixed oscillatory strain of 0.2%. The linear variation of the shear rate was assessed from 0.1 to 100 Hz at 25°C using a rotational mode. The recovery of the mechanical properties was performed under a continuous strain sweep with alternating small oscillation force (1% strain for 60 s) and a large force (500% strain for 40 s) with a fixed frequency of 10 Hz at 25°C.

2.3 | Conductivity measurements

The resistance values were measured with an Inductance, Capacitance and Resistance (LCR) meter (TH2830). The resistivity was calculated using the resistance by the following formula: $\rho = RS/L$, where R is the resistance of the sample, and S and L represent the cross-sectional area and length of the sample, respectively. Therefore, the conductivity (σ) could be calculated through $\sigma = 1/\rho$.

Cell culture and cytotoxicity assay. RAW 264.7 cells were purchased from iCell Bioscience Inc., collected and counted following resuscitation. In a 12-well plate, the cell suspension concentration was increased to 2×10^4 cells/well. For 12 h, the cells were cultured at 5% CO_2 and 37°C to ensure adhesion to the wall. Following 30 min of UV sterilization, the Ca-PAA-CNF-MXene hydrogels were clamped into the orifice plate and cultivated for an additional 72 h. The original medium was then removed and added to a 500 μl 10% Cell Counting Kit-8 medium for a further 2 h of culture. Finally, the cell survival rate was determined using a full wavelength marker enzyme (optical density = 450), followed by fluorescence photography.

Characterization. X-ray diffraction (XRD) was used to characterize MAX and MXene powders, as well as Ca-PAA, Ca-PAA-CNF, and Ca-PAA-CNF-MXene hydrogels. The XRD patterns were recorded using a PANalytical-Empyrean X-ray diffractometer equipped with Cu Kα radiation ($\lambda = 1.54$ Å) with scanning at a rate of $4° \text{ min}^{-1}$. Double-sided carbon conductive tape was used to attach freeze-dried foams of Ca-PAA, Ca-PAA-CNF, and Ca-PAA-CNF-MXene hydrogels to an aluminum scanning sample stub, and microscopic morphological images were observed using a field emission scanning electron microscope (Zeiss Ultra Plus). Transmission electron microscopy and selected area electron diffraction (SAED) were used to investigate the microstructures of MXene (JEOL-7100F). An atomic force microscope was also used to measure the thickness of MXene (Bruker Dimension ICON). The functional groups of SDBS, MXene, PAA, Ca-PAA, Ca-PAA-CNF, and Ca-PAA-CNF-MXene were analyzed and identified utilizing a Fourier-transform infrared (FTIR)

2767441x, 2022, 4, Downloaded from https://onlinelibrary.wiley.com/doi/10.1002/idm2.12026 by Universitätsbibliothek Basel, Wiley Online Library on [02/11/2022]. See the Terms and Conditions (https://onlinelibrary.wiley.com/terms-and-conditions) on Wiley Online Library for rules of use; OA articles are governed by the applicable Creative Commons License

spectrometer (Thermo Nicolet Nexus) with a wavelength range of 4000–400 cm^{-1}. The weight loss of MXene, PAA, Ca-PAA, Ca-PAA-CNF, and Ca-PAA-CNF-MXene was evaluated by thermal gravimetric analysis (TGA; NETZSCH STA449F3 Jupiter) at a heating rate of 10°C min^{-1} in an air environment from room temperature to 800°C. The chemical bonds of MXene, Ca-PAA-CNF, and Ca-PAA-CNF-MXene hydrogels were studied employing X-ray photoelectron spectroscopy (XPS) on an Axis Ultra DLD Kratos AXIS SUPRA spectrometer. Ca-PAA-CNF-MXene hydrogels were printed in three dimensions using a 3D bioprinter (Bio-X; Cellink). An LCR meter (TH2830) operated by LabView software collected all relative resistance change signals. The hydrogels with a dimension of 22.86 mm × 10.16 mm (length × width) were prepared to measure the EMI SE in the frequency range of 8.2–12.4 GHz (X-band) via a waveguide method in a vector network analyzer (VNA, NYSE: A N5244A). The S-parameters were recorded and employed to calculate the SE_T, SE_A, and SE_R for each sample.

3 | RESULTS AND DISCUSSION

3.1 | Preparation and structural characterization of Ca-PAA-CNF-MXene hydrogels

A 3D printable Ca-PAA-CNF-MXene composite hydrogel was synthesized, as schematically illustrated in Figure 1A. Firstly, $Ti_3C_2T_x$ MXene nanosheets were produced through a selective etch of the Al layers in Ti_3AlC_2 MAX with LiF and HCl, followed by ultrasonic treatment to generate delaminated MXene (d-MXene) nanosheets (Figure S1A). The matching SAED pattern in Figure S1B shows the hexagonal structure of d-MXene at the atomic level. The geometrical characteristics of d-MXene were investigated using atomic force microscopy in Figure S1C, manifesting an ultrathin thickness (1.5 nm). The comparison of the XRD patterns of MAX and the produced MXene nanosheets (Figure 1B) suggested that the characteristic peak (002) moved from 9.72° to 5.92° and the peak at

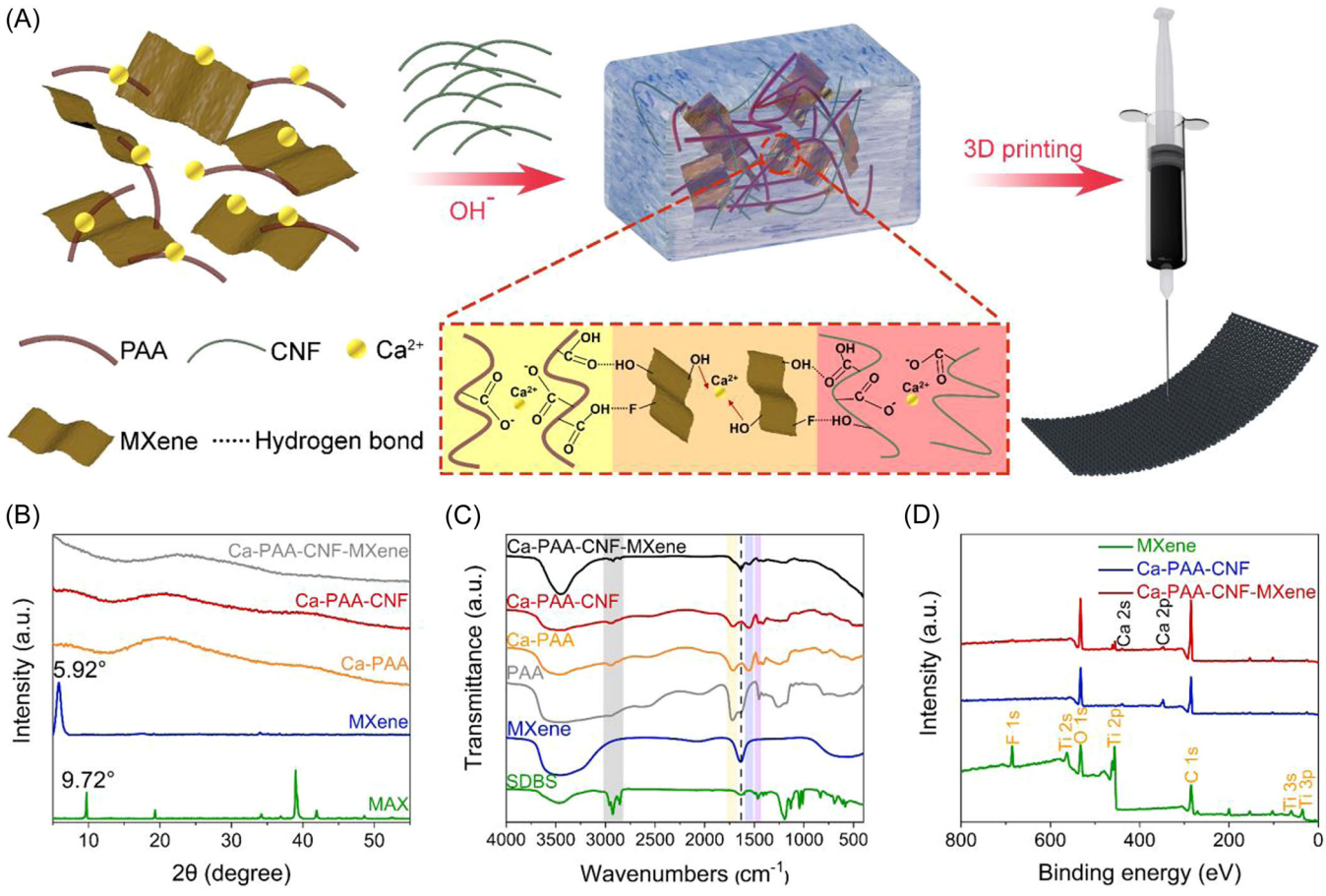

FIGURE 1 Preparation and structural characterization of Ca-PAA-CNF-MXene composite hydrogels. (A) Schematic illustration of preparing and 3D printing Ca-PAA-CNF-MXene hydrogels. (B) XRD patterns, (C) FTIR spectra, and (D) XPS surveys of Ca-PAA-CNF-MXene hydrogels and the corresponding reference samples. CNF, cellulose nanofibers; FTIR, Fourier-transform infrared; PAA, polyacrylic acid; XPS, X-ray photoelectron spectroscopy; XRD, X-ray diffraction

2767441x, 2022, 4, Downloaded from https://onlinelibrary.wiley.com/doi/10.1002/idm2.12026 by Universitätsbibliothek Basel, Wiley Online Library on [02/11/2022]. See the Terms and Conditions (https://onlinelibrary.wiley.com/terms-and-conditions) on Wiley Online Library for rules of use; OA articles are governed by the applicable Creative Commons License

39° weakened. Thereby the layer spacing was proved to expand, confirming the production of MXene.[44] Thereafter, Ca-PAA-CNF-MXene composite hydrogels were easily synthesized, exploiting the one-step procedure inspired by mussel secretions that are formed by byssus fibers through protein–metal coordination mediated by 3,4-dihydroxyphenylalanine).[45] To this end, a NaOH aqueous solution containing a small volume of CNF was dropwise added to a mixture of $CaCl_2$, PAA, and MXene containing a small amount of SDBS and incubated for 1 h with vigorous stirring, leading to the formation of a black sticky hydrogel. The Ca-PAA, Ca-PAA-CNF, and Ca-PAA-CNF-MXene hydrogels all exhibited amorphous phases, except a small peak visible at the small angle (5°) of Ca-PAA-CNF-MXene, indicating the presence of MXene (Figure 1B). Without the addition of CNF, the freeze-dried Ca-PAA hydrogel shows a reasonably smooth surface and large pore diameters (8–16 μm) (Figure S2A). Particularly, with the addition of CNF, the Ca-PAA-CNF and Ca-PAA-CNF-MXene hydrogel exhibited abundant homogeneous and dense pores of sizes ranging from 1.8 to 3.6 μm (Figure S2B,C). This significantly enhances the specific surface area and thereby capacity to hold water and form abundant hydrogen bonds for the CNF-based hydrogels, which are instrumental in the stability and durability of the hydrogels in electromechanical sensing applications.

The molecular structure of SDBS, MXene, PAA, Ca-PAA, Ca-PAA-CNF, and Ca-PAA-CNF-MXene were analyzed utilizing FTIR (Figure 1C). The peaks of 1714 and 1452 cm^{-1} in the light yellow and light purple areas, respectively, were ascribed to the PAA backbone's stretching vibration (−CO of −COOH) and in-plane bending vibration (–CH of $–CH_2$).[46] The peaks at 1554 cm^{-1} produced by Ca-PAA, Ca-PAA-CNF, and Ca-PAA-CNF-MXene relating to PAA suggest the chelating interaction between $–COO^-$ and Ca^{2+} marked as the light blue area in the spectra (Figure 1C). Additionally, the peaks at 2854, 2926, and 2960 cm^{-1}, correspond to ν_s (CH_2), ν_{as} (CH_2), and ν_{as} (CH_3), respectively, of SDBS (a light gray area, Figure 1C).[47] Similarly, distinctive peaks of SDBS were detected in the spectra of Ca-PAA, Ca-PAA-CNF, and Ca-PAA-CNF-MXene hydrogels, indicating that SDBS was effectively integrated into the hydrogels. Notably, the spectrum of MXene contains a significant amount of OH at 3455 cm^{-1} and a C=O stretching vibration at 1630 cm^{-1}. The spectra of Ca-PAA-CNF-MXene show a peak at the dotted line (1630 cm^{-1}), suggesting the presence of MXene in the Ca-PAA-CNF-MXene hydrogel. Compared to Ca-PAA and Ca-PAA-CNF hydrogels, the strong and broad peak around 3455 cm^{-1} shows that the Ca-PAA-CNF-MXene hydrogel has more hydrogen bonds. The chemical composition of the samples was evaluated using XPS (Figure 1D). Ca-PAA-CNF-MXene exhibits higher C and O signals in the XPS survey spectrum than both MXene and Ca-PAA-CNF, demonstrating that Ca-PAA-CNF-MXene has more oxygen-containing groups required for hydrogel cross-linking. Ca-PAA-CNF-MXene shows the same Ti 2p peak as MXene in Figure S3A,D, suggesting that MXene retained its structure throughout the preparation procedure, correlating to the XRD pattern (Figure 1B). Moreover, TGA accurately verified the composition of the different composite hydrogels (Figure S4).

The formation process of the Ca-PAA-CNF-MXene hydrogels, schematically shown in Figure 1A relies on several supramolecular interactions. Numerous carboxyl groups on the PAA chain can chelate with Ca^{2+} to form hydrogel frameworks. Additionally, carboxyl groups on the carboxylated CNF chain can also interact with Ca^{2+} further to form ionic cross-linked structures. Furthermore, hydroxyl and fluoride ions on the surface of MXene may establish supramolecular interactions and hydrogen bonds with PAA, CNF, and Ca^{2+}, leading to the formation of a robust hydrogel network structure.

3.2 | Multifunctional performance of Ca-PAA-CNF-MXene hydrogels

The rheological properties of the composite hydrogels were characterized using oscillatory rheology (Figure 2). As exhibited in a frequency varying from 0.1 to 10 Hz with a fixed strain of 0.2%, the loss modulus (G'') of Ca-PAA and Ca-PAA-MXene (7.5%) exceeds the storage modulus (G') thus indicating that the material is behaving in a liquid-like state, meanwhile, the G' of Ca-PAA-CNF and Ca-PAA-CNF-MXene (7.5%) (the mass of MXene is relative to the mass of PAA) exceed the G'' displaying a solid-like state (Figure 2A). Therefore, the addition of CNF enables the hydrogels to form a more complex network structure, resulting in a more solid-like behavior without causing the collapse of the structure. At the same time, the rheological tests of the Ca-PAA-CNF-MXene hydrogels with different content of MXene are presented in Figure 2B. The G' of the samples were greater than G'', and the G', G'' of the composite hydrogels rose with an increasing MXene content. Besides, the viscosity relationships of Ca-PAA, Ca-PAA-MXene, Ca-PAA-CNF, and Ca-PAA-CNF-MXene with increasing shear rates were also investigated (Figure 2C). These hydrogels all exhibited shear-thinning properties. Furthermore, Ca-PAA-CNF-MXene hydrogels with different contents of MXene also manifested shear-thinning properties (Figure 2D). However, the suitable viscosity for 3D extrusion printing

2767441x, 2022, 4, Downloaded from https://onlinelibrary.wiley.com/doi/10.1002/idm2.12026 by Universitätsbibliothek Basel, Wiley Online Library on [02/11/2022]. See the Terms and Conditions (https://onlinelibrary.wiley.com/terms-and-conditions) on Wiley Online Library for rules of use; OA articles are governed by the applicable Creative Commons License

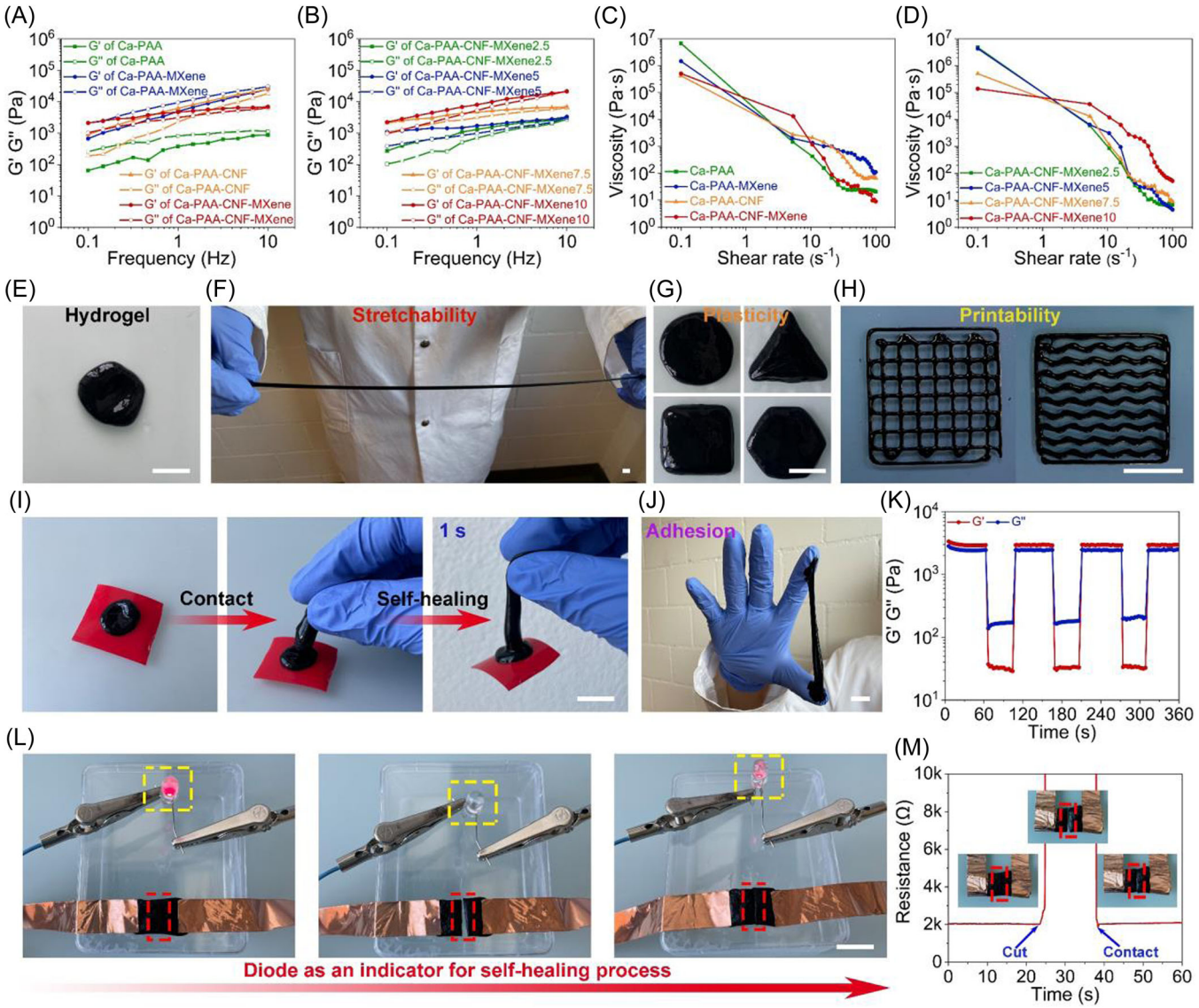

FIGURE 2 Frequency dependencies of storage modulus (G') and loss modulus (G'') for (A) Ca-PAA, Ca-PAA-MXene, Ca-PAA-CNF, and Ca-PAA-CNF-MXene, and (B) Ca-PAA-CNF-MXene hydrogels with different MXene content. Viscosities of (C) Ca-PAA, Ca-PAA-MXene, Ca-PAA-CNF, Ca-PAA-CNF-MXene hydrogels, and (D) Ca-PAA-CNF-MXene hydrogels with different MXene content, as a function of shear rate. (E) Photograph of prepared Ca-PAA-CNF-MXene hydrogel. Photographs show the (F) stretchability, (G) plasticity, (H) printability, (I) fast self-healing capability, and (J) adhesivity of the Ca-PAA-CNF-MXene hydrogels. (K) Cyclic strain sweeps of Ca-PAA-CNF-MXene hydrogels. Self-healing processes of Ca-PAA-CNF-MXene hydrogels (L) with a diode used as an indicator, and (M) the real-time resistance changes. All scale bars are 1 cm. CNF, cellulose nanofibers; PAA, polyacrylic acid

should be 0.1–10 Pa s.[48–50] In addition, a great 3D printing ink also needs to meet the requirements of $G' > G'' > 1000$ Pa in the low-frequency region, so as to maintain the 3D shape without collapse after extrusion.[20] Therefore, the subsequent Ca-PAA-CNF-MXene hydrogels used for printing contained 7.5 wt% MXene.

The black adhesive Ca-PAA-CNF-MXene composite hydrogel is a gum-like material with multifunctional properties (Figure 2E). It can be easily stretched to more than 1000% of its original length without breaking (Figure 2F). In addition, the composite hydrogel is highly plastic and can be molded into any desired shape, such as round, triangle, square, or hexagon (Figure 2G). This excellent plasticity can be useful in various applications such as wearable devices. Moreover, the composite hydrogel is also 3D printable and can be extruded into, for example, grid and ripple patterns, expanding its customized applications as flexible wearables (Figure 2H, Movies S1 and S2). The composite hydrogel additionally shows adhesion and self-healing ability (Figure 2I). When one piece of hydrogel was

2767441x, 2022, 4, Downloaded from https://onlinelibrary.wiley.com/doi/10.1002/idm2.12026 by Universitätsbibliothek Basel, Wiley Online Library on [02/11/2022]. See the Terms and Conditions (https://onlinelibrary.wiley.com/terms-and-conditions) on Wiley Online Library for rules of use; OA articles are governed by the applicable Creative Commons License

contacted with another piece of hydrogel placed on an acrylic elastomer (VHB 4905, 3 M), the two pieces of hydrogel would self-heal in less than 1 s. At the same time, the hydrogel can vertically stick between two fingers without falling, further confirming its good adhesive performance (Figure 2J). The self-healing ability of the composite hydrogel was further characterized by cyclic strain sweeps in Figure 2K. When the composite hydrogel was subjected to small amplitude oscillating shear strain (1%) for 60 s, G' was slightly greater than G'', indicating that the hydrogel displayed viscoelasticity and suggesting that elasticity was slightly dominant. When the oscillating shear strain increased to 500% and lasted for 40 s, the values of G' and G'' significantly decreased, showing a larger G'' than G'. Thereby the network structure of hydrogel was destroyed, and its solid-like properties were lost. When the strain recovered to 1%, the two moduli immediately recovered to their original levels, conferring that the hydrogel network structure had self-repaired. Furthermore, a light-emitting diode was employed to assess the self-healing processes of the Ca-PAA-CNF-MXene composite hydrogel (length × width × thickness: 1 cm × 1 cm × 0.1 cm) (Figure 2L). When the diode, wires, power supply, and hydrogel were connected to form a loop, the diode emitted red light. When the hydrogel was cut, the diode was turned off. As soon as the cut hydrogel was again brought into contact, the diode lit up again. The corresponding quantitative characterization was investigated in Figure 2M. The resistance value of the composite hydrogel returned to the original 2 kΩ when contacting, displaying its rapid self-healing ability. The biocompatibility of hydrogels was also quantitatively analyzed in Figure S5. The 72-h survival rate of RAW 264.7 cells cultured on the hydrogel was over 93.7%, suggesting that the hydrogel has the potential to be used in wearable devices. Furthermore, this hydrogel disintegrated after 1 day in phosphate buffer saline buffer in Figure S6, displaying the potential for matrix biodegradation and potential recycling of the MXene materials required for the development of more environmentally friendly electronics.

3.3 | Multiple sensing capabilities of MXene composite hydrogel-based sensor

Based on the above analyses, Ca-PAA-CNF-MXene is a multifunctional conductive hydrogel with biocompatibility, self-healing, matrix disintegrability, and adhesion properties. It can also respond to deformation, yielding resistance changes. These functions are necessary for the further development of environmentally friendly wearable electronics. To demonstrate this, a multifunctional sensor was fabricated by two VHB sandwiching a layer of printed Ca-PAA-CNF-MXene hydrogel connected with copper wires as shown in the schematic Figure 3A. VHB can not only prevent hydrogel from evaporating water but also be stably applied to various parts of the body (for instance, finger, wrist, and forehead) for movement monitoring (Figure S7). Once the Ca-PAA-CNF-MXene sensor was stretched to an elongation (ε), the relative resistance changes ($\Delta R/R_0$) would also increase (Figure 3B). After fitting the data, the $\Delta R/R_0$ was estimated according to the following equation:

$$\Delta R/R_0 = 0.0026\varepsilon^2 + 1.9018\varepsilon. \quad (1)$$

Therefore, the gauge factor (GF) followed the formula:

$$\mathrm{GF} = 0.0026\varepsilon + 1.9018. \quad (2)$$

It then follows that, when the sensor was stretched to 100%, the GF was 2.16. In addition, the $\Delta R/R_0$ under different strain levels were measured to evaluate the reliability of the sensor under different deformation levels. When the strain sensor in Figure 3C, was stretched to 25%, 50%, 100%, and 200%, the corresponding $\Delta R/R_0$ was about 49.7%, 103.8%, 217.1%, and 488.0%, respectively, which corresponded to the curve in Figure 3B. Furthermore, the cyclic stability of the strain sensor was also investigated in Figure 3D. When the fixed tensile strain was 100%, the relative resistance of the strain sensor could keep stable after the repeated stretching for 10 min. In addition, the multifunctional sensor can be applied to the throat to sense vocals for the detection of deformation as a strain sensor. Different words were pronounced differently, so the throat stimulated the voice sensor accordingly, yielding different signals. When speaking "Hi," "Wuhan," "OK," and "No," the voice sensor responded with a completely different but stable relative resistance change signal (Figure 3E–H). Besides, the multifunctional sensor can function as a smart writing keyboard to sense signatures on its surface when coated with two layers of polyethylene terephthalate films. When the English letters "W," "U," and "T" were written on the signature sensor, the sensor can respond with signals in different forms (Figure 3I–K). When the sentence "ILOVEYOU" was continuously written, it accurately distinguished different English letters by different output signals (Figure 3L). Noteworthily, the two signals of the letter "O" were very similar, which manifested the stability of the signature sensor. The international Morse code can represent 26 English alphabet letters in different combinations of dots and dashes (Figure 3M).[51] Therefore, the

2767441x, 2022, 4, Downloaded from https://onlinelibrary.wiley.com/doi/10.1002/idm2.12026 by Universitätsbibliothek Basel, Wiley Online Library on [02/11/2022]. See the Terms and Conditions (https://onlinelibrary.wiley.com/terms-and-conditions) on Wiley Online Library for rules of use; OA articles are governed by the applicable Creative Commons License

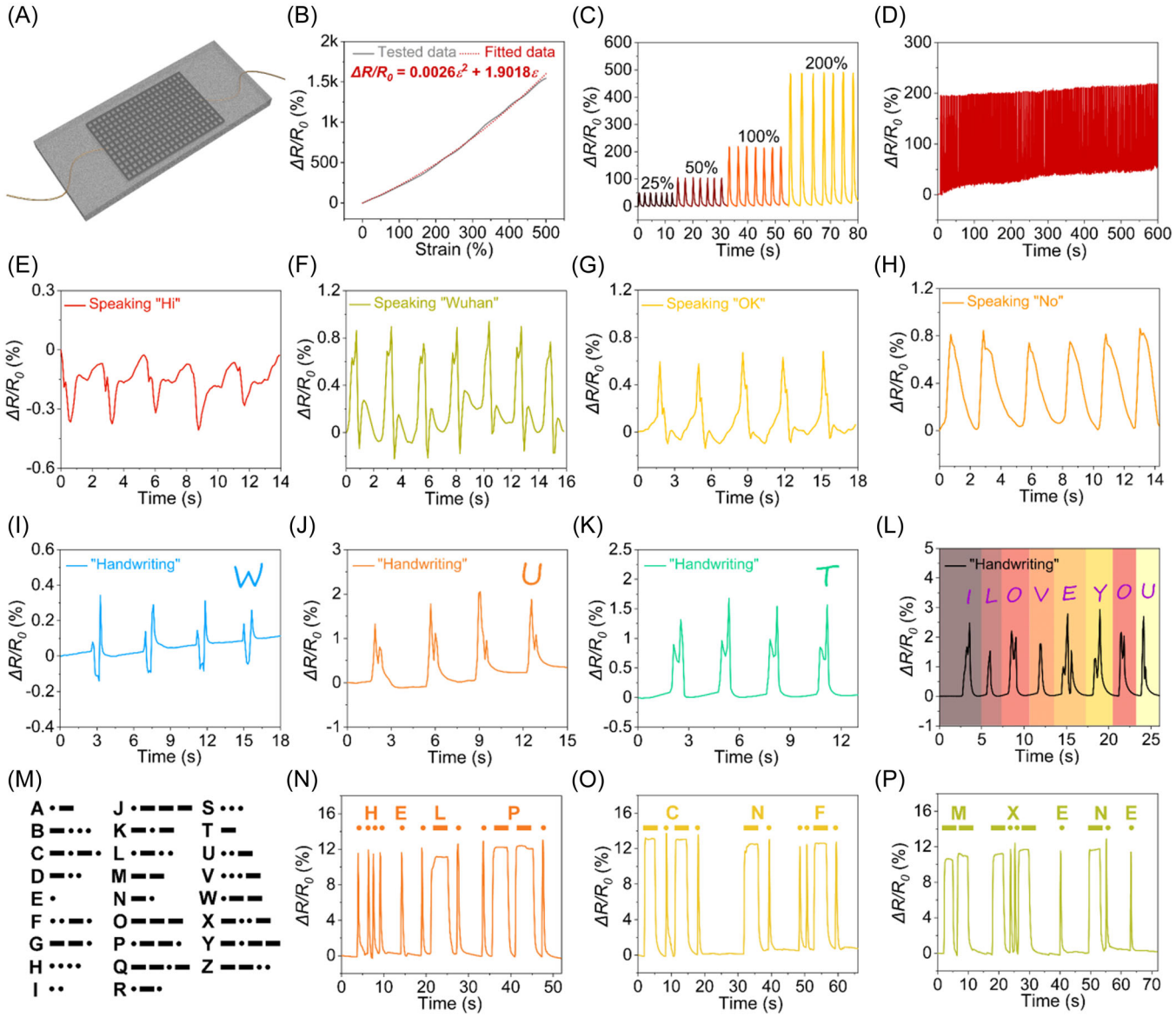

FIGURE 3 Monitoring processes of Ca-PAA-CNF-MXene hydrogel as a multifunctional sensor. (A) Schematic illustration of a sandwiched Ca-PAA-CNF-MXene sensor. (B) Tested and fitted curves of the relative resistance changes as a function of tensile deformation. (C) Relative resistance changes of the sensor under different strain. (D) Cyclic test of the sensor under 80% strain. Ca-PAA-CNF-MXene sensor, attached to the throat, real-time monitoring speaking (E) "Hi," (F) "Wuhan," (G) "OK," and (H) "No." Ca-PAA-CNF-MXene hydrogel sandwiched by two layers of PET films, real-time monitoring handwriting English letters of (I) "W," (J) "U," (K) "T," and (L) "ILOVEYOU." (M) Schematic diagram of 26 English letters corresponding to Morse code symbols. Through the relative resistance change signals responding to the decoding of (N) "HELP," (O) "CNF," and (P) "MXene." CNF, cellulose nanofibers; PAA, polyacrylic acid; PET, polyethylene terephthalate

multifunctional sensor was attached to the index finger for the evaluation, and consequently, the written dots can be represented by short-range $\Delta R/R_0$ signals. In contrast, dashes can be represented by long-range $\Delta R/R_0$ signals.[52] Hence, the Morse code can be edited and transmitted remotely by using body movements. Hence, some words, such as "HELP," "CNF," and "MXENE," were compiled and transmitted by finger bending (Figure 3N–P).

3.4 | EMI shielding performances of MXene composite hydrogels

In addition to electromechanical sensing, the flexible, conductive, and porous Ca-PAA-CNF-MXene hydrogels can display efficient EMI shielding properties. EMI shielding materials are highly desirable for the electromagnetic compatibility of electronics and human health protection against electromagnetic pollution or

2767441x, 2022, 4, Downloaded from https://onlinelibrary.wiley.com/doi/10.1002/idm2.12026 by Universitätsbibliothek Basel, Wiley Online Library on [02/11/2022]. See the Terms and Conditions (https://onlinelibrary.wiley.com/terms-and-conditions) on Wiley Online Library for rules of use; OA articles are governed by the applicable Creative Commons License

interference.[53,54] EMI shielding effectiveness (SE) manifests the attenuation capability of the EMI shielding monoliths. Generally, a commercial SE value of 20 dB corresponding to a 99% attenuation of the incident electromagnetic waves is necessary.[55–58] Increasing MXene contents can gradually increase the electrical conductivity due to the formed MXene conductive paths in the hydrogels (Figure 4A), which improves the EMI SE. Without integrating the conductive MXene nanosheets, the EMI SE of the hydrogels is relatively low due to a lack of MXene based conductive paths (Figure 4B). However, it is well understood that polar water molecules can also interact with electromagnetic waves, transforming their energy into heat energy.[59,60] Consequently, the 1.5-mm-thick hydrogels without embedded MXene still show EMI SE values of around 14 dB. Furthermore, we have also measured the shielding by reflection (SE_R) and absorption (SE_A) to better show the EMI shielding mechanism (Figure 4C). The total SE (SE_T) is the sum of the SE_A and SE_R, influenced by the electric dipoles and mobile charge carriers, respectively.[54,57,58,61] Therefore, the conductive and polarization losses derived from the MXene conductive paths will benefit the enhanced absorption of the incident electromagnetic waves, thus improving the SE_A and SE_T of the composite hydrogels (Figure 4D).[62,63] Moreover, the interfaces between the highly conductive MXenes and insulating polymer matrices in the hydrogel lead to a strong interfacial polarization under the electric field of incident electromagnetic waves, further improving the SE_A.[61–63] Furthermore, the porous structure of the hydrogels is instrumental in increasing the multiple reflections of electromagnetic waves, leading to more interactions between the waves and MXene embedded cell walls (Figure 4D).[61–64] This further increases the EMI SE. Therefore, both the SE_A and SE_T increase significantly by increasing MXene mass ratios in the hydrogels, for example, SE_T can reach up to 25 dB with a dominant SE_A of 20 dB for the 10 wt% MXene embedded composite hydrogels. Thus, taken together, the synergistic coactions of conductive MXene paths, the porous structure, the interfaces between MXene and polymer matrices, and the internal water-rich condition all play crucial roles in improving the EMI shielding performance of the composite hydrogels.

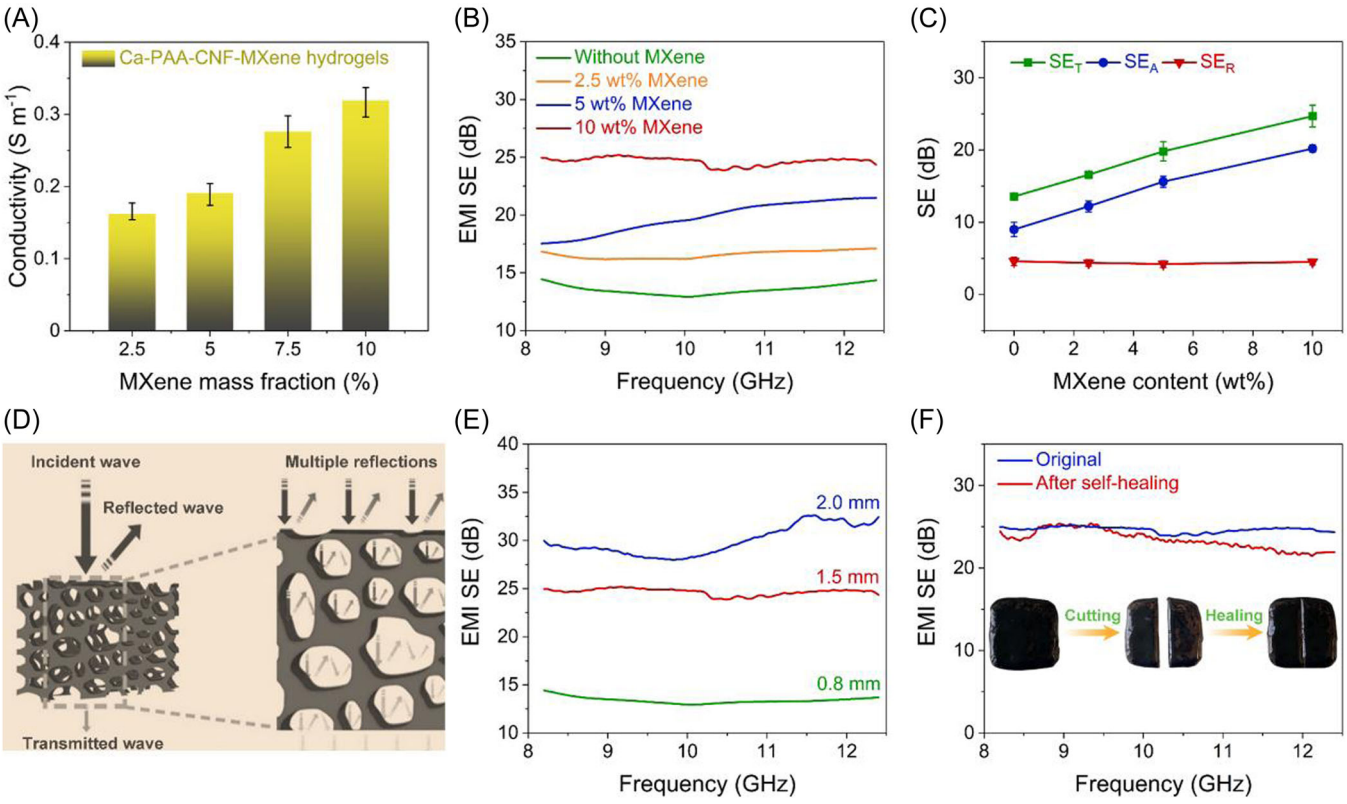

FIGURE 4 (A) The conductivity, (B) X-band EMI SE, and (C) SE_T, SE_A, SE_R at a thickness of 1.5 mm of the Ca-PAA-CNF-MXene composite hydrogels with various MXene mass fractions. (D) The illustration of the porous structure of the composite hydrogels on the EMI shielding performance. X-band EMI SE of (E) the 10 wt% MXene composite hydrogels at various thicknesses, and (F) the hydrogel before and after the self-healing process. CNF, cellulose nanofibers; EMI, electromagnetic interference; PAA, polyacrylic acid; SE, shielding effectiveness

2767441x, 2022, 4, Downloaded from https://onlinelibrary.wiley.com/doi/10.1002/idm2.12026 by Universitätsbibliothek Basel, Wiley Online Library on [02/11/2022]. See the Terms and Conditions (https://onlinelibrary.wiley.com/terms-and-conditions) on Wiley Online Library for rules of use; OA articles are governed by the applicable Creative Commons License

Apart from the MXene contents in the composite hydrogels, the thickness of the samples can also be effortlessly controlled and used to further adjust the EMI SE. For instance, the EMI SE of the composite hydrogels with 10 wt% MXene can reach more than 30 dB, corresponding to an attenuation of more than 99.9% of the incident electromagnetic waves, at a thickness of 2.0 mm (Figure 4E). Moreover, it is intriguing that the self-healing composite hydrogels can still retain the EMI SE after the sample is self-healed from two pieces, which cannot be accomplished by other EMI shielding monoliths, such as aerogels or bulk materials (Figure 4F).[58,61–64] This efficiently illustrates the high potential of our flexible, self-healing, and porous composite hydrogels as high-performance and durable EMI shielding materials for next-generation electronics. Combined with the facile printing technique, the bioinspired multifunctional hydrogel has both sensing and electromagnetic shielding properties, thereby manifesting the potential for its development and application in multifunctional intelligent materials.

4 | CONCLUSION

This study presented a facile approach to prepare a bioinspired Ca-PAA-CNF-MXene hydrogel formed by physical and chemical bonding between PAA, CNF, MXene, and calcium ions. This hydrogel exhibited an extensive combination of functional properties, including stretchability, plasticity, adhesion, 3D printability, self-healing, biocompatibility, and electrical conductivity. Based on these properties, the hydrogel has application potential in multifunctional intelligent devices. A layer of printed Ca-PAA-CNF-MXene hydrogel on copper electrodes can concurrently serve as a strain sensor, a voice sensor, a signature sensor, and a Morse code transmitter that can sensitively and stably respond to external stimuli. Additionally, the porous structure of the intelligent hydrogel distinguishes itself with an efficient EMI shielding performance, potentially contributing to protecting human beings from electromagnetic radiation. Based on the above functions, this bioinspired multifunctional hydrogel manifests a considerable application prospect in the field of intelligent wearable devices.

AUTHOR CONTRIBUTIONS

Jingjiang We conceived experimental ideas, performed the experiment, analyzed data, drew figures, and wrote the manuscript. Chenglong Zhu prepared experimental materials, conducted experiments, and collected data. Zhihui Zeng conceived experimental ideas, performed experiment, characterization, analysis, writing the electromagnetic interference part. Fei Pan suggested characterizing methods and contributed to data analysis and interpretation (chemical and physical structures). Fuqiang Wan conducted partial experiments. Liwen Lei collected and analyzed partial data. Gustav Nyström reviewed and edited draft. Zhengyi Fu conceived experimental ideas, supervized the conduct of the experiment and provided experimental funding.

ACKNOWLEDGMENTS

Jingjiang Wei and Chenglong Zhu contributed equally to this study. The author Jingjiang Wei gratefully acknowledges the financial support from China Scholarship Council (CSC, File No. 202006950043). This study has been financially supported by the National Natural Science Foundation of China (Grant Nos. 51521001, 51832003, 51911530153).

CONFLICT OF INTEREST

The authors declare no conflict of interest.

ORCID

Jingjiang Wei http://orcid.org/0000-0001-8513-6510
Fei Pan http://orcid.org/0000-0002-9801-5619

REFERENCES

[1] Studart AR. Additive manufacturing of biologically-inspired materials. *Chem Soc Rev*. 2016;45:359-376.
[2] Wegst UG, Bai H, Saiz E, Tomsia AP, Ritchie RO. Bioinspired structural materials. *Nat Mater*. 2015;14:23-36.
[3] Meyers MA, McKittrick J, Chen P-Y. Structural biological materials: critical mechanics-materials connections. *Science*. 2013;339:773-779.
[4] Studart AR. Towards high-performance bioinspired composites. *Adv Mater*. 2012;24:5024-5044.
[5] Xie J, Ping H, Tan T, et al. Bioprocess-inspired fabrication of materials with new structures and functions. *Prog Mater Sci*. 2019;105:100571.
[6] Wei J, Ping H, Xie J, et al. Bioprocess-inspired microscale additive manufacturing of multilayered TiO_2/polymer composites with enamel-like structures and high mechanical properties. *Adv Funct Mater*. 2020;30:1904880.
[7] Xie J, Xie H, Su BL, et al. Mussel-directed synthesis of nitrogen-doped anatase TiO_2. *Angew Chem Int Ed*. 2016;55:3031-3035.
[8] Silverman HG, Roberto FF. Understanding marine mussel adhesion. *Mar Biotechnol*. 2007;9:661-681.
[9] Waite JH, Andersen NH, Jewhurst S, Sun C. Mussel adhesion: finding the tricks worth mimicking. *J Adhes*. 2005;81:297-317.
[10] Burke SA, Ritter-Jones M, Lee BP, Messersmith PB. Thermal gelation and tissue adhesion of biomimetic hydrogels. *Biomed Mater*. 2007;2:203-210.
[11] Venkatesh S, Sizemore SP, Byrne ME. Biomimetic hydrogels for enhanced loading and extended release of ocular therapeutics. *Biomaterials*. 2007;28:717-724.

2767441x, 2022, 4, Downloaded from https://onlinelibrary.wiley.com/doi/10.1002/idm2.12026 by Universitätsbibliothek Basel, Wiley Online Library on [02/11/2022]. See the Terms and Conditions (https://onlinelibrary.wiley.com/terms-and-conditions) on Wiley Online Library for rules of use; OA articles are governed by the applicable Creative Commons License

[12] Sant S, Hancock MJ, Donnelly JP, Iyer D, Khademhosseini A. Biomimetic gradient hydrogels for tissue engineering. *Can J Chem Eng*. 2010;88:899-911.
[13] Wang R, Li J, Chen W, et al. A biomimetic mussel-inspired ε-poly-l-lysine hydrogel with robust tissue-anchor and anti-infection capacity. *Adv Funct Mater*. 2017;27:1604894.
[14] Le X, Lu W, Zhang J, Chen T. Recent progress in biomimetic anisotropic hydrogel actuators. *Adv Sci*. 2019;6:1801584.
[15] Zhang C, Wu B, Zhou Y, Zhou F, Liu W, Wang Z. Mussel-inspired hydrogels: from design principles to promising applications. *Chem Soc Rev*. 2020;49:3605-3637.
[16] Fan H, Gong JP. Fabrication of bioinspired hydrogels: challenges and opportunities. *Macromolecules*. 2020;53:2769-2782.
[17] Li L, Smitthipong W, Zeng H. Mussel-inspired hydrogels for biomedical and environmental applications. *Polym Chem*. 2015;6:353-358.
[18] Xie C, Wang X, He H, Ding Y, Lu X. Mussel-inspired hydrogels for self-adhesive bioelectronics. *Adv Funct Mater*. 2020;30:1909954.
[19] Grigoryan B, Paulsen SJ, Corbett DC, et al. Multivascular networks and functional intravascular topologies within biocompatible hydrogels. *Science*. 2019;364:458-464.
[20] Müller LA, Zimmermann T, Nyström G, Burgert I, Siqueira G. Mechanical properties tailoring of 3D printed photoresponsive nanocellulose composites. *Adv Funct Mater*. 2020;30:2002914.
[21] Wang Q, Sun J, Yao Q, Ji C, Liu J, Zhu Q. 3D printing with cellulose materials. *Cellulose*. 2018;25:4275-4301.
[22] Athukoralalage SS, Balu R, Dutta NK, Roy, Choudhury N. 3D bioprinted nanocellulose-based hydrogels for tissue engineering applications: a brief review. *Polymers*. 2019;11:898.
[23] Kim D-H, Viventi J, Amsden JJ, et al. Dissolvable films of silk fibroin for ultrathin conformal bio-integrated electronics. *Nat Mater*. 2010;9:511-517.
[24] Velasco-Hogan A, Xu J, Meyers MA. Additive manufacturing as a method to design and optimize bioinspired structures. *Adv Mater*. 2018;30:1800940.
[25] Aeby X, Poulin A, Siqueira G, Hausmann MK, Nyström G. Fully 3D printed and disposable paper supercapacitors. *Adv Mater*. 2021;33:2101328.
[26] Paul R, Zhai Q, Roy AK, Dai L. Charge transfer of carbon nanomaterials for efficient metal-free electrocatalysis. *Interdiscip Mater*. 2022;1:28-50.
[27] Jiang J, Liu J. Iron anode-based aqueous electrochemical energy storage devices: recent advances and future perspectives. *Interdiscip Mater*. 2022;1:116-139.
[28] Xiong F, Jiang Y, Cheng L, et al. Low-strain TiP_2O_7 with three-dimensional ion channels as long-life and high-rate anode material for Mg-ion batteries. *Interdiscip Mater*. 2022;1:140-147.
[29] Kanda H, Dan Mihailetchi V, Gueunier-Farret ME, et al. Three-terminal perovskite/integrated back contact silicon tandem solar cells under low light intensity conditions. *Interdiscip Mater*. 2022;1:148-156.
[30] Lei Z, Wu P. Zwitterionic skins with a wide scope of customizable functionalities. *ACS Nano*. 2018;12:12860-12868.
[31] Hu Y, Zhuo H, Zhang Y, et al. Graphene oxide encapsulating liquid metal to toughen hydrogel. *Adv Funct Mater*. 2021;31:2106761.
[32] Xu X, Ozden S, Bizmark N, Arnold CB, Datta SS, Priestley RD. A bioinspired elastic hydrogel for solar-driven water purification. *Adv Mater*. 2021;33:2007833.
[33] Zhao Z, Fang R, Rong Q, Liu M. Bioinspired nanocomposite hydrogels with highly ordered structures. *Adv Mater*. 2017;29:1703045.
[34] Ghadban A, Ahmed AS, Ping Y, et al. Bioinspired pH and magnetic responsive catechol-functionalized chitosan hydrogels with tunable elastic properties. *Chem Commun*. 2016;52:697-700.
[35] Han M, Shuck CE, Rakhmanov R, et al. Beyond $Ti_3C_2T_x$: MXenes for electromagnetic interference shielding. *ACS Nano*. 2020;14:5008-5016.
[36] Zhang Y-Z, Lee KH, Anjum DH, et al. MXenes stretch hydrogel sensor performance to new limits. *Sci Adv*. 2018;4:eaat0098.
[37] Zhang Y, Gong M, Wan P. MXene hydrogel for wearable electronics. *Matter*. 2021;4:2655-2658.
[38] Kuila D, Blay GA, Borjas RE, et al. Polyacrylic acid (poly-A) as a chelant and dispersant. *J Appl Polym Sci*. 1999;73:1097-1115.
[39] Yang X, Biswas SK, Han J, et al. Surface and interface engineering for nanocellulosic advanced materials. *Adv Mater*. 2021;33:2002264.
[40] Wei J, Xie J, Zhang P, et al. Bioinspired 3D printable, self-healable, and stretchable hydrogels with multiple conductivities for skin-like wearable strain sensors. *ACS Appl Mater Interfaces*. 2021;13:2952-2960.
[41] Wei J, Wan F, Zhang P, et al. Bioprocess-inspired synthesis of printable, self-healing mineral hydrogels for rapidly responsive, wearable ionic skin. *Chem Eng Sci*. 2021;424:130549.
[42] Sun S, Mao LB, Lei Z, Yu SH, Cölfen H. Hydrogels from amorphous calcium carbonate and polyacrylic acid: bioinspired materials for mineral plastics. *Angew Chem Int Ed*. 2016;55:11765-11769.
[43] Lei Z, Wang Q, Sun S, Zhu W, Wu P. A bioinspired mineral hydrogel as a self-healable, mechanically adaptable ionic skin for highly sensitive pressure sensing. *Adv Mater*. 2017;29:1700321.
[44] Firestein KL, vonTreifeldt JE, Kvashnin DG, et al. Young's modulus and tensile strength of Ti_3C_2 MXene nanosheets as revealed by in situ TEM probing, AFM nanomechanical mapping, and theoretical calculations. *Nano Lett*. 2020;20:5900-5908.
[45] Priemel T, Palia G, Förste F, et al. Microfluidic-like fabrication of metal ion-cured bioadhesives by mussels. *Science*. 2021;374:206-211.
[46] Anjum S, Gurave PM, Gupta B. Calcium ion-induced self-healing pattern of chemically crosslinked poly (acrylic acid) hydrogels. *Polym Int*. 2018;67:250-257.
[47] Potapova E, Jolsterå R, Holmgren A, Grahn M. In-situ spectroscopic study of surfactant adsorption onto hematite from binary mixtures and the effect of inorganic ions. *Surf Interface Anal*. 2014;46:1110-1114.
[48] Zhu F, Cheng L, Yin J, et al. 3D printing of ultratough polyion complex hydrogels. *ACS Appl Mater Interfaces*. 2016;8:31304-31310.
[49] Tian K, Bae J, Bakarich SE, et al. 3D printing of transparent and conductive heterogeneous hydrogel-elastomer systems. *Adv Mater*. 2017;29:1604827.

2767441x, 2022, 4, Downloaded from https://onlinelibrary.wiley.com/doi/10.1002/idm2.12026 by Universitätsbibliothek Basel, Wiley Online Library on [02/11/2022]. See the Terms and Conditions (https://onlinelibrary.wiley.com/terms-and-conditions) on Wiley Online Library for rules of use; OA articles are governed by the applicable Creative Commons License

[50] Lei Z, Wang Q, Wu P. A multifunctional skin-like sensor based on a 3D printed thermo-responsive hydrogel. *Mater Horiz*. 2017;4:694-700.
[51] Yu Z, Wu P. Underwater communication and optical camouflage ionogels. *Adv Mater*. 2021;33:2008479.
[52] Cheng B, Wu P. Scalable fabrication of Kevlar/$Ti_3C_2T_x$ MXene intelligent wearable fabrics with multiple sensory capabilities. *ACS Nano*. 2021;15:8676-8685.
[53] Shahzad F, Alhabeb M, Hatter CB, et al. Electromagnetic interference shielding with 2D transition metal carbides (MXenes). *Science*. 2016;353:1137-1140.
[54] Zeng Z, Jiang F, Yue Y, et al. Flexible and ultrathin waterproof cellular membranes based on high-conjunction metal-wrapped polymer nanofibers for electromagnetic interference shielding. *Adv Mater*. 2020;32:1908496.
[55] Yang Y, Gupta MC, Dudley KL, Lawrence RW. Novel carbon nanotube-polystyrene foam composites for electromagnetic interference shielding. *Nano Lett*. 2005;5:2131-2134.
[56] Yang Y, Gupta MC, Dudley KL, Lawrence RW. Conductive carbon nanofiber-polymer foam structures. *Adv Mater*. 2005;17:1999-2003.
[57] Chen Z, Xu C, Ma C, Ren W, Cheng HM. Lightweight and flexible graphene foam composites for high-performance electromagnetic interference shielding. *Adv Mater*. 2013;25:1296-1300.
[58] Thomassin J-M, Jerome C, Pardoen T, Bailly C, Huynen I, Detrembleur C. Polymer/carbon based composites as electromagnetic interference (EMI) shielding materials. *Mater Sci Eng R Rep*. 2013;74:211-232.
[59] Song WL, Zhang YJ, Zhang KL, et al. Ionic conductive gels for optically manipulatable microwave stealth structures. *Adv Sci*. 2020;7:1902162.
[60] Zhu Y, Liu J, Guo T, Wang JJ, Tang X, Nicolosi V. Multifunctional $Ti_3C_2T_x$ MXene composite hydrogels with strain sensitivity toward absorption-dominated electromagnetic-interference shielding. *ACS Nano*. 2021;15:1465-1474.
[61] Zeng Z, Wu T, Han D, Ren Q, Siqueira G, Nyström G. Ultralight, flexible, and biomimetic nanocellulose/silver nanowire aerogels for electromagnetic interference shielding. *ACS Nano*. 2020;14:2927-2938.
[62] Zeng Z, Wang C, Siqueira G, et al. Nanocellulose-MXene biomimetic aerogels with orientation-tunable electromagnetic interference shielding performance. *Adv Sci*. 2020;7:2000979.
[63] Zhao S, Zhang H-B, Luo J-Q, et al. Highly electrically conductive three-dimensional $Ti_3C_2T_x$ MXene/reduced graphene oxide hybrid aerogels with excellent electromagnetic interference shielding performances. *ACS Nano*. 2018;12:11193-11202.
[64] Song Q, Ye F, Yin X, et al. Carbon nanotube–multilayered graphene edge plane core-shell hybrid foams for ultrahigh-performance electromagnetic-interference shielding. *Adv Mater*. 2017;29:1701583.

SUPPORTING INFORMATION

Additional supporting information can be found online in the Supporting Information section at the end of this article.

How to cite this article: Wei J, Zhu C, Zeng Z, et al. Bioinspired cellulose-integrated MXene-based hydrogels for multifunctional sensing and electromagnetic interference shielding. *Interdiscip Mater*. 2022;1:495-506. doi:10.1002/idm2.12026

2767441x, 2022, 4, Downloaded from https://onlinelibrary.wiley.com/doi/10.1002/idm2.12026 by Universitätsbibliothek Basel, Wiley Online Library on [02/11/2022]. See the Terms and Conditions (https://onlinelibrary.wiley.com/terms-and-conditions) on Wiley Online Library for rules of use; OA articles are governed by the applicable Creative Commons License